Effects of Two-Stage Cold Rolling Schedule on Microstructure and Texture Evolution of Strip Casting Grain-Oriented Silicon Steel with Extra-Low Carbon

HONG-YU SONG, HAI-TAO LIU, WEN-QIANG LIU, YIN-PING WANG, ZHEN-YU LIU, and GUO-DONG WANG

A 0.27 mm-thick grain-oriented silicon steel sheet with extra-low carbon was successfully produced by a novel processing route including strip casting, normalizing, two-stage cold rolling with an intermediate annealing, primary annealing, and secondary recrystallization annealing. The evolutions of microstructure and texture along the whole processing route were investigated with a special emphasis on the effects of two-stage cold rolling schedule. It was found that Goss orientation originated in the first cold rolling due to shear banding and relatively strong Goss texture evolved through the whole thickness after intermediate annealing. This is significantly different from the results in conventional process in which the origin of Goss texture is in the hot rolling stage and Goss texture only develops below the sheet surface. Besides, it was found that cold rolling schedule had significant influences on microstructure homogeneity, evolution of λ-fiber texture in primary annealed state and, thus, on secondary recrystallization. In case of appropriate cold rolling schedule, a homogeneous microstructure with Goss texture, relatively strong γ-fiber texture and medium α-fiber texture was observed in the primary annealed strip. Although Goss texture in primary annealed state was much weaker than that in two-stage route in conventional process, a perfect secondary recrystallization microstructure was produced and the magnetic induction B_8 was as high as 1.85 T. By contrast, when the cold rolling schedule was inappropriate, the primary annealed strips exhibited inhomogeneous microstructure, together with weak γ-fiber texture, medium α-fiber and λ-fiber texture. Finally, the sheets showed incomplete secondary recrystallization microstructure in which a large number of fine grains still existed.

DOI: 10.1007/s11661-016-3334-9

I. INTRODUCTION

GRAIN-ORIENTED silicon steel is mainly used in transformers due to its excellent magnetic properties originating from sharp $\{110\}\langle001\rangle$ preferred orientation (Goss texture).[1] Although the manufacturing process has been well developed since Goss first proposed the technological approach in 1934,[2] the conventional manufacturing process is still complicated.[3] Twin-roll strip casting is based on the concept originally proposed by Bessemer[4] and characterized by a significantly high heat exaction capacity.[5] It can eliminate the thick slab casting and reduce hot rolling passes by supplying as-cast strips with thickness close to the conventional hot rolled sheets.[6] The recent progress in strip casting provides a possibility of producing grain-oriented silicon steels by a simpler process than conventional process. However, the evolutions of microstructure, texture, and inhibitor along strip casting route may be greatly different from those along the conventional processing routes due to its initial rapidly solidified microstructure and limited hot rolling reduction.

Dunn[7] first pointed out secondary recrystallization as the responsible process for the formation of sharp Goss texture in grain-oriented silicon steel. The following researchers[8] confirmed that the presences of Goss orientation and a fine dispersion of precipitates in the primary recrystallization matrix are requisite for secondary recrystallization. It has been well accepted that the origin of Goss orientation in primary recrystallization matrix is in the hot rolling stage, where Goss orientation develops below the sheet surface due to shear deformation[9,10] arising from heavy hot rolling reduction exceeding 95 pct. Böttcher *et al.*[11] demonstrated the importance of Goss orientation generated in hot rolling by experiments in which the removal of Goss-containing layer resulted in incomplete secondary recrystallization. Besides, it was considered that lots of fine inhibitors were generated during the multi-pass hot rolling with heavy reduction.[12] Hence, hot rolling has a critical influence on the manufacturing of grain-oriented silicon steels in conventional process. By contrast, the as-cast strips are produced directly from the melt in strip

HONG-YU SONG, Ph.D. Student, HAI-TAO LIU, Associate Professor, WEN-QIANG LIU and YIN-PING WANG, Graduate Students, and ZHEN-YU LIU and GUO-DONG WANG, Professors, are with the State Key Laboratory of Rolling and Automation, Northeastern University, Shenyang 110819, P.R. China. Contact e-mail: liuht@ral.neu.edu.cn

Manuscript submitted February 24, 2015.
Article published online January 20, 2016

casting processing route.[13–15] Thus, the initial solidification microstructure and texture may be significantly different from those of conventional casting slabs and hot rolled sheets in conventional process. Besides, given that the thickness of the as-cast strip is close to that of hot rolled strip, the total hot rolling reduction is very limited. The origin of Goss texture may be restricted due to the lack of shear deformation during hot rolling. As a result, the development of Goss texture during secondary recrystallization annealing may be affected and it may be considerably distinct from that in conventional process. However, the corresponding researches have been rarely reported.

In this paper, a 0.27 mm-thick grain-oriented silicon steel sheet with extra-low carbon was produced based on a novel processing route including strip casting, normalizing, two-stage cold rolling with an intermediate annealing, primary annealing, and secondary recrystallization annealing. Different cold rolling schedules were applied to investigate their influences on microstructure and texture evolution and, thus, on secondary recrystallization.

II. EXPERIMENTAL METHODS

The composition of tested steel was (mass pct) 0.0026 C, 3.32 Si, 0.064 Mn, 0.024 S, 0.035 Al, 0.0093 N, and balance Fe. Strip casting experiment of 2.3 mm-thick as-cast strip was carried out using a vertical type twin-roll caster, as described in detail in previous literatures.[16,17] The as-cast strip was soaked at 1223 K (950 °C) for 4 minutes and quenched by cold water. Then, three different processing routes were adopted: (R1) The normalized strip was first cold rolled to 1.0 mm with 56.5 pct reduction, intermediate annealed at 1103 K (830 °C) for 3 minutes, finally cold rolled to 0.27 mm with 73 pct reduction and primary annealed at 1103 K (830 °C) for 3 minutes. Finally, the primary annealed strip was heated to 1473 K (1200 °C) from 1073 K (800 °C) at a heating rate of 20 K/h (20 °C/h) in the atmosphere of 100pctN_2 and then kept at 1473 K (1200 °C) for 10 hours; (R2) The normalized strip was first cold rolled to 0.8 mm with 65.2 pct reduction, intermediate annealed at 1103 K (830 °C) for 3 minutes, finally cold rolled to 0.27 mm with 66.3 pct reduction and followed by the same primary annealing and secondary recrystallization annealing with route R1; (R3) The normalized strip was first cold rolled to 0.6 mm with 73.9 pct reduction, intermediate annealed at 1103 K (830 °C) for 3 min, finally cold rolled to 0.27 mm with 55 pct reduction and followed the same primary annealing and secondary recrystallization annealing with route R1. The schematic diagram of the processing was shown in Figure 1. For convenience, the samples were denoted as first cold rolled (FCR) strip, intermediate annealed (IA) strip, secondary cold rolled (SCR) strip, primary annealed (PA) strip, and secondary recrystallization annealed (SRA) strip.

Metallographic specimens were machined, polished and etched with 4 pct nital. A LEICA-DMIRM optical microscopy was applied on longitudinal sections as defined by the rolling direction (RD) and normal direction (ND). The crystallographic textures were determined by measuring three incomplete pole figures {110}, {200}, and {211} in the back reflection mode in a Bruker D8 Discover X-ray diffractometer with $Co_{K\alpha 1}$ radiation. The measured layer is defined as the parameter $S = 2a/d$, where a and d are the distances from the center and sheet thickness, respectively. The specimens used for texture measurements were prepared with the size of 22 mm (L) × 20 mm (W). Electron backscattered diffraction (EBSD) system equipped at a ZEISS ULTRA 55 field emission scanning electron microscope (SEM) was performed to analyze the crystallography characteristics of specimens. The observation of precipitates was conducted in a TECNAI G2 F20 transmission electron microscope (TEM) equipped with an energy dispersive X-ray spectroscopy.

The measurement of the magnetic induction at 800 A/m (B_8) and core loss at 1.7 T and 50 Hz ($P_{1.7/50}$) were performed by means of a single sheet tester under alternating current (AC). The tester contained a modular magnetic measurement instrument based on a data acquisition unit with an adapted software package for data analysis. The magnetic field was obtained by integrating the voltage pick up loop and the locking of magnetic induction peak was achieved by digital feedback. The core loss was obtained using voltammetry and digital integration method. In order to save materials, nonstandard custom-built permeameter was applied in the tester. The sample used for measuring magnetic properties was 100 mm (rolling direction) in length and 30 mm (transverse direction) in width. The tester used in this work has been calibrated to make the measurement comparable to the stand testing.

III. RESULTS

A. *Microstructure and Texture of As-Cast Strip*

The as-cast strip was composed of coarse columnar ferrite grains (see Figure 2(a)), and the texture was characterized by strong λ-fiber texture ($\langle 001\rangle \| ND$) (see Figure 2(b)). The microstructure and texture of the as-cast strip was quite similar to the results by Liu *et al.*[15]

B. *Microstructure and Texture Evolution Through Processing*

After normalizing, the microstructure and texture were quite similar to those of the as-cast strip. After first cold rolling, a remarkably inhomogeneous deformation microstructure was produced, as shown in Figures 3(a), 4(a), and 5(a). The microstructure was composed of two types of deformed grains, *i.e.*, the rough and smooth grains. The rough grains showed lots of in-grain shear bands, while the smooth ones exhibited little sign of deformation. The texture was mainly characterized by strong λ-fiber texture, strong α-fiber texture ($\langle 110\rangle$//RD), and relatively weak γ-fiber texture ($\langle 111\rangle$//ND) with the maximum at $\{111\}\langle 110\rangle$ component, as shown

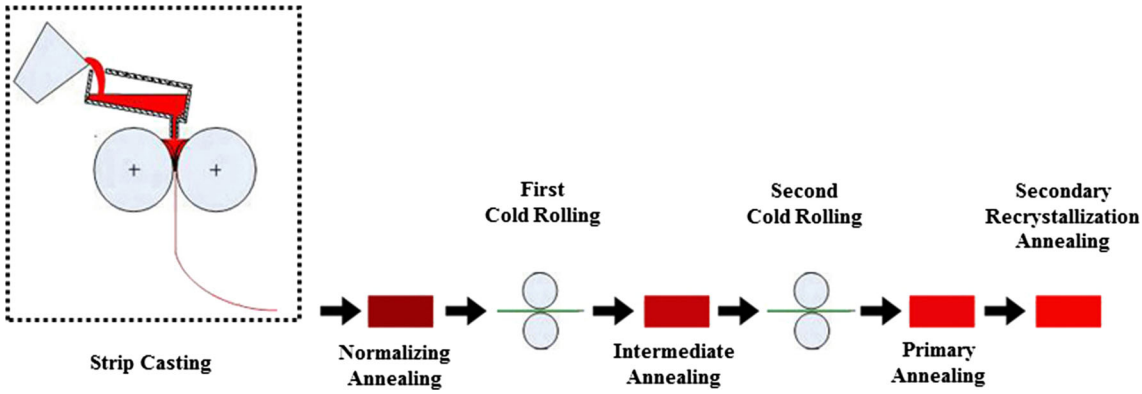

Fig. 1—Schematic diagram of the processing for the tested steel.

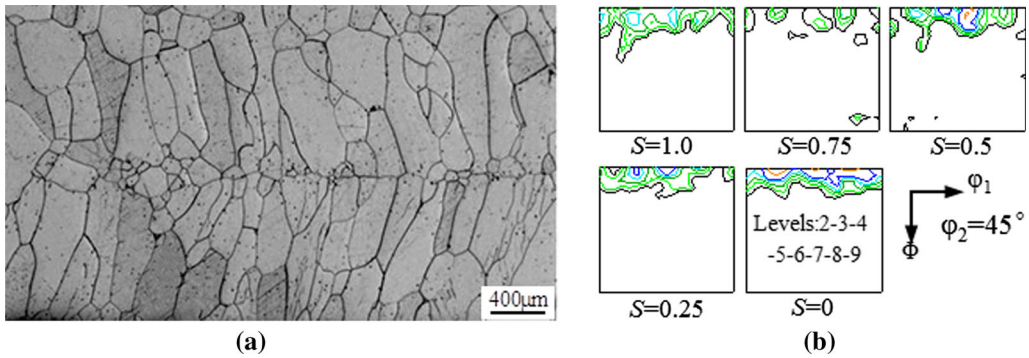

Fig. 2—Optical microstructure (*a*) and texture (*b*) of the as-cast strip.

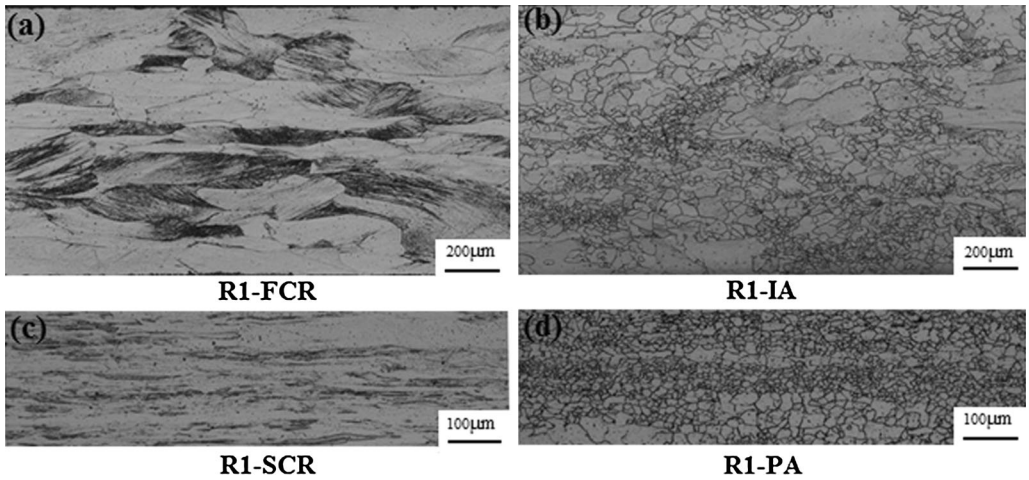

Fig. 3—Through-thickness optical microstructures of the strips which were processed by route R1. (*a*) First cold rolled strip, (*b*) intermediate annealed strip, (*c*) second cold rolled strip, and (*d*) primary annealed strip.

in Figures 6(a), 7(a), and 8(a). After intermediate annealing, the strips showed a remarkable inhomogeneous microstructure in which fine grains and large grains co-existed, as shown in Figures 3(b), 4(b), and 5(b). It should be noted that many banded colonies composed of fine grains were observed through the whole thickness. The texture was mainly characterized by medium λ-fiber texture, strong α-fiber texture, relatively weak γ-fiber texture and medium Goss texture through thickness, as shown in Figures 6(b), 7(b), and 8(b).

After second stage cold rolling, a relatively homogeneous deformation microstructure was produced, as shown in Figures 3(c), 4(c), and 5(c). The texture was mainly characterized by strong α-fiber texture, medium λ-fiber texture and strong γ-fiber texture with the maximum at $\{111\}\langle 112\rangle$ component through thickness, as shown in Figures 6(c), 7(c), and 8(c). After primary

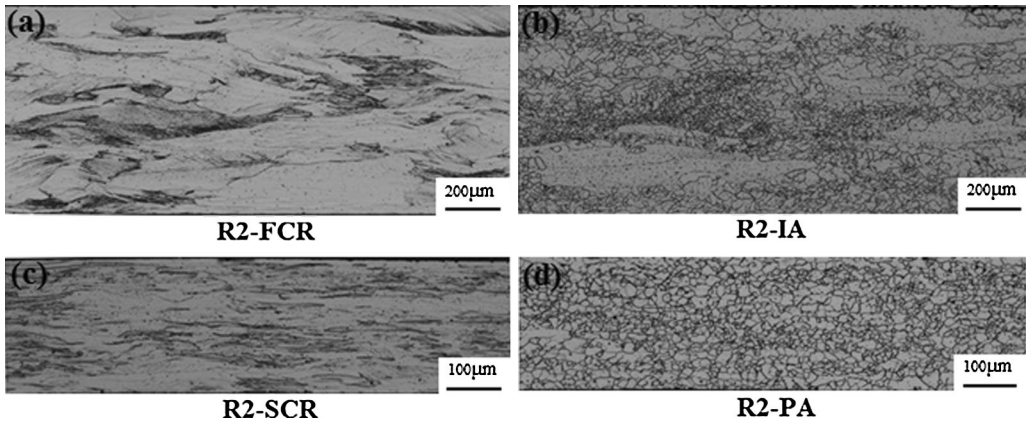

Fig. 4—Through-thickness optical microstructures of the strips which were processed by route R2. (*a*) First cold rolled strip, (*b*) intermediate annealed strip, (*c*) second cold rolled strip, and (*d*) primary annealed strip.

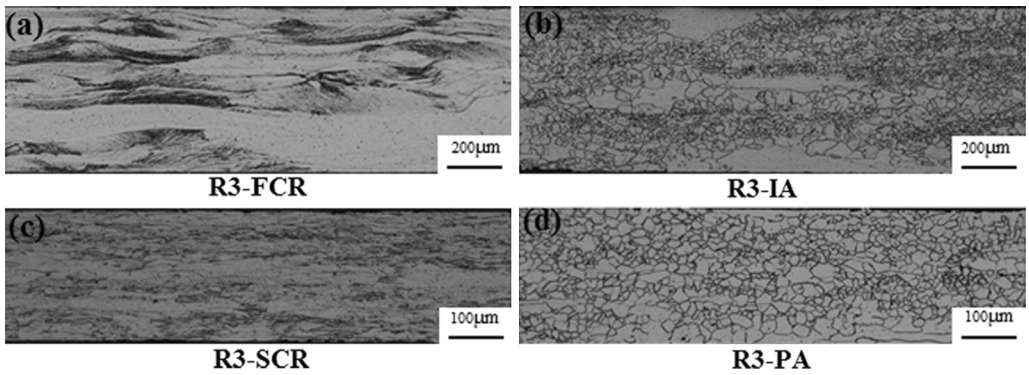

Fig. 5—Through-thickness optical microstructures of the strips which were processed by route R3. (*a*) First cold rolled strip, (*b*) intermediate annealed strip, (*c*) second cold rolled strip, and (*d*) primary annealed strip.

annealing, a homogeneous recrystallization microstructure composed of equiaxed grains was produced (see Figure 4(d)) and the texture was characterized by Goss texture, relatively strong γ-fiber texture and medium α-fiber texture (see Figure 7(d)). By contrast, some large elongated grains evolved near the surface in Figures 3(d) and 5(d) and the textures showed medium α-fiber texture, medium γ-fiber texture and weak λ-fiber texture, as shown in Figures 6(d) and 8(d).

C. *Inhibitors in As-Cast and Normalized Strip*

Figure 9 shows, the inhibitors in as-cast strip. It was observed that the inhibitors in as-cast strip were mainly co-precipitates of AlN and MnS and the size range of inhibitors was 10 to 30 nm. Figure 10 shows, the inhibitors in the normalized strip. It was found that, after normalizing, the precipitates were still mainly co-precipitates of AlN and MnS. However, the size of the inhibitors was slightly increased.

D. *Microstructure and Magnetic Properties of Secondary Recrystallized Strip*

Figure 11 shows, the microstructures of secondary recrystallized strips. As shown, the strips adopted by different processing routes exhibited distinct microstructures. The R2-SRA sample showed perfect secondary recrystallization microstructure, while the other two strips exhibited incomplete secondary recrystallization microstructures in which a large number of fine grains were observed. It should be noted that the large grains in R1-SRA and R3-SRA strips were all elongated along the rolling direction. It was measured that the magnetic induction B_8 of R2-SRA sample was as high as 1.85 T, while the values of the other two strips were below 1.75 T. And, the core loss of R2-SRA sample was 1.43 W/kg, while the values of the other two strips were above 2.0 W/kg.

IV. DISCUSSION

A. *Inhibitor Evolution Through Processing*

Grain-oriented silicon steels usually contain 0.04 to 0.08 mass pct C and 2.9 to 3.2 mass pct Si. This leads to the co-existence of ferrite and austenite during hot rolling and normalizing in which MnS and AlN precipitates are formed due to the changing solubility product during temperature decreasing and γ/α transformation.[8,18] By contrast, the tested steel in this work remained in ferrite phase through whole processing route due to extra-low carbon. Besides, the as-cast strip was produced by strip

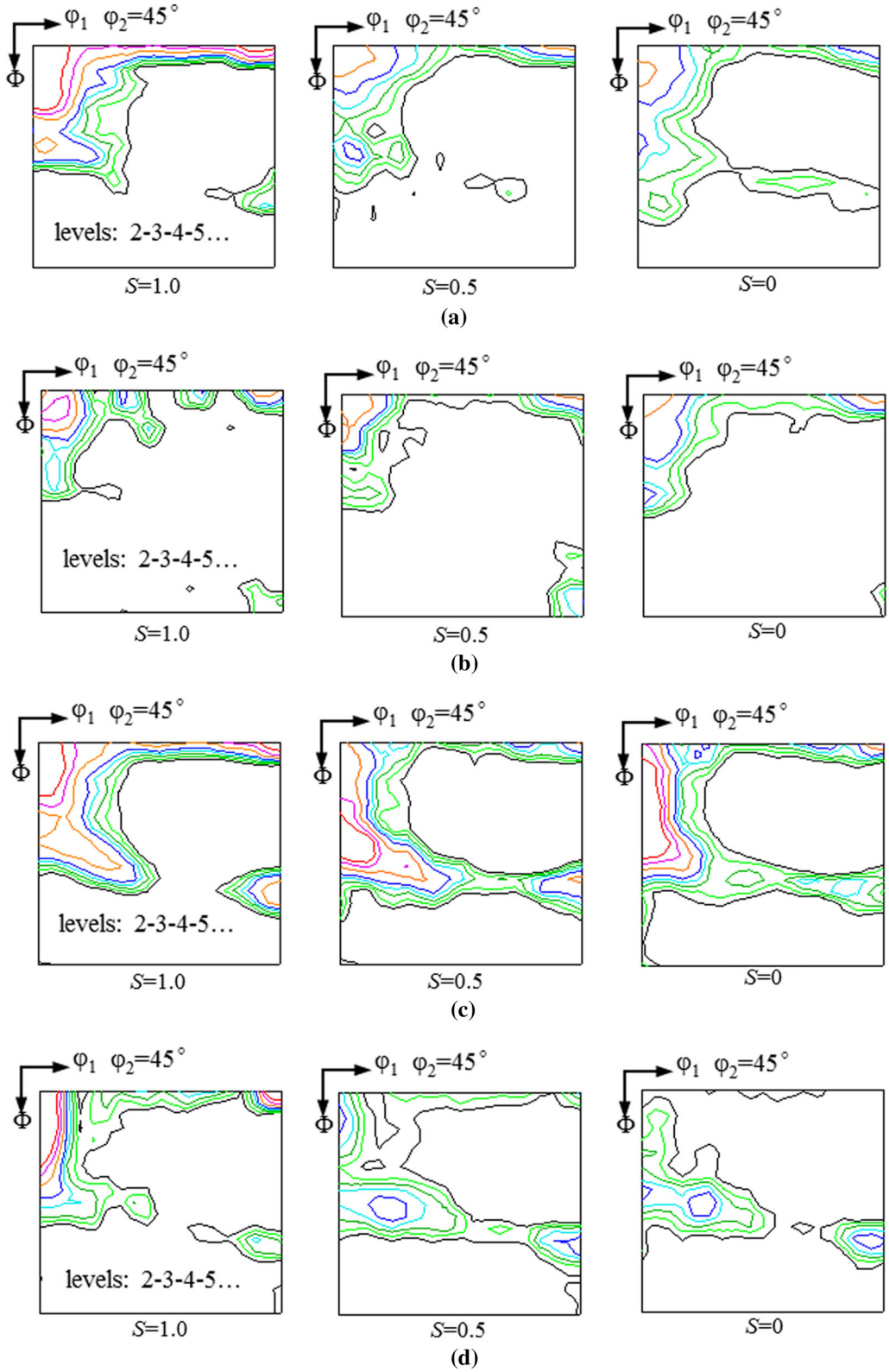

Fig. 6—Through-thickness textures (φ_2 = 45 deg section) of the strips which were processed by route R1. (*a*) First cold rolled strip, (*b*) intermediate annealed strip, (*c*) second cold rolled strip, and (*d*) primary annealed strip.

casting, and hot rolling was eliminated in the processing route. Hence, the evolution of inhibitors may be different from that in conventional process.

The inhibitor forming elements may remain in solid solution state just after solidification because solidification in strip casting can be completed within 1 seconds

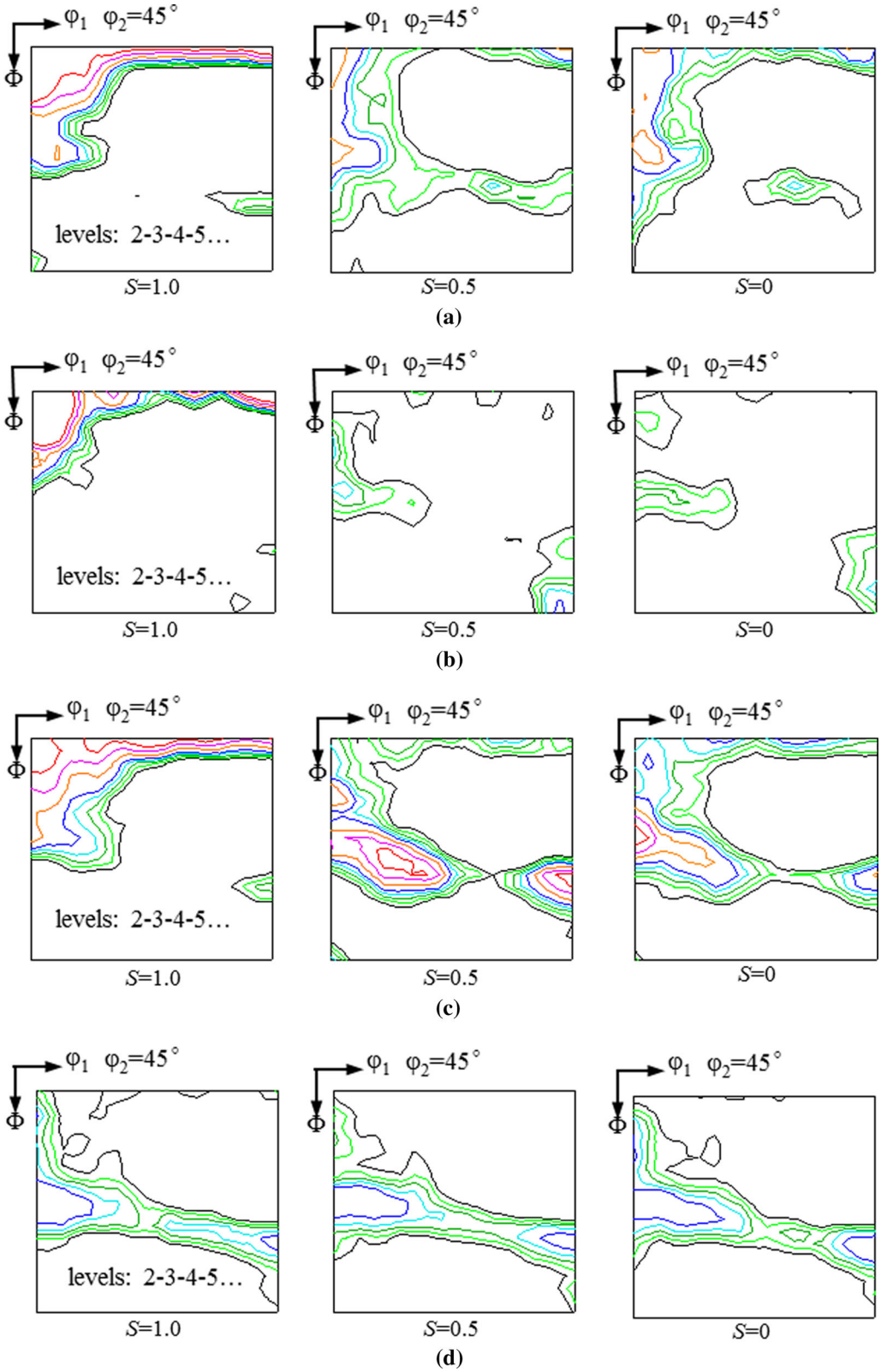

Fig. 7—Through-thickness textures (φ_2 = 45 deg section) of the strips which were processed by route R2. (*a*) First cold rolled strip, (*b*) intermediate annealed strip, (*c*) second cold rolled strip, and (*d*) primary annealed strip.

due to high heat extraction capacity.[5] After solidification, inhibitors may be formed during the following cooling process. In this work, it was calculated that the temperature required for complete dissolution of AlN in ferrite was higher than that of MnS. Thus, AlN may precipitate earlier than MnS during the air-cooling after

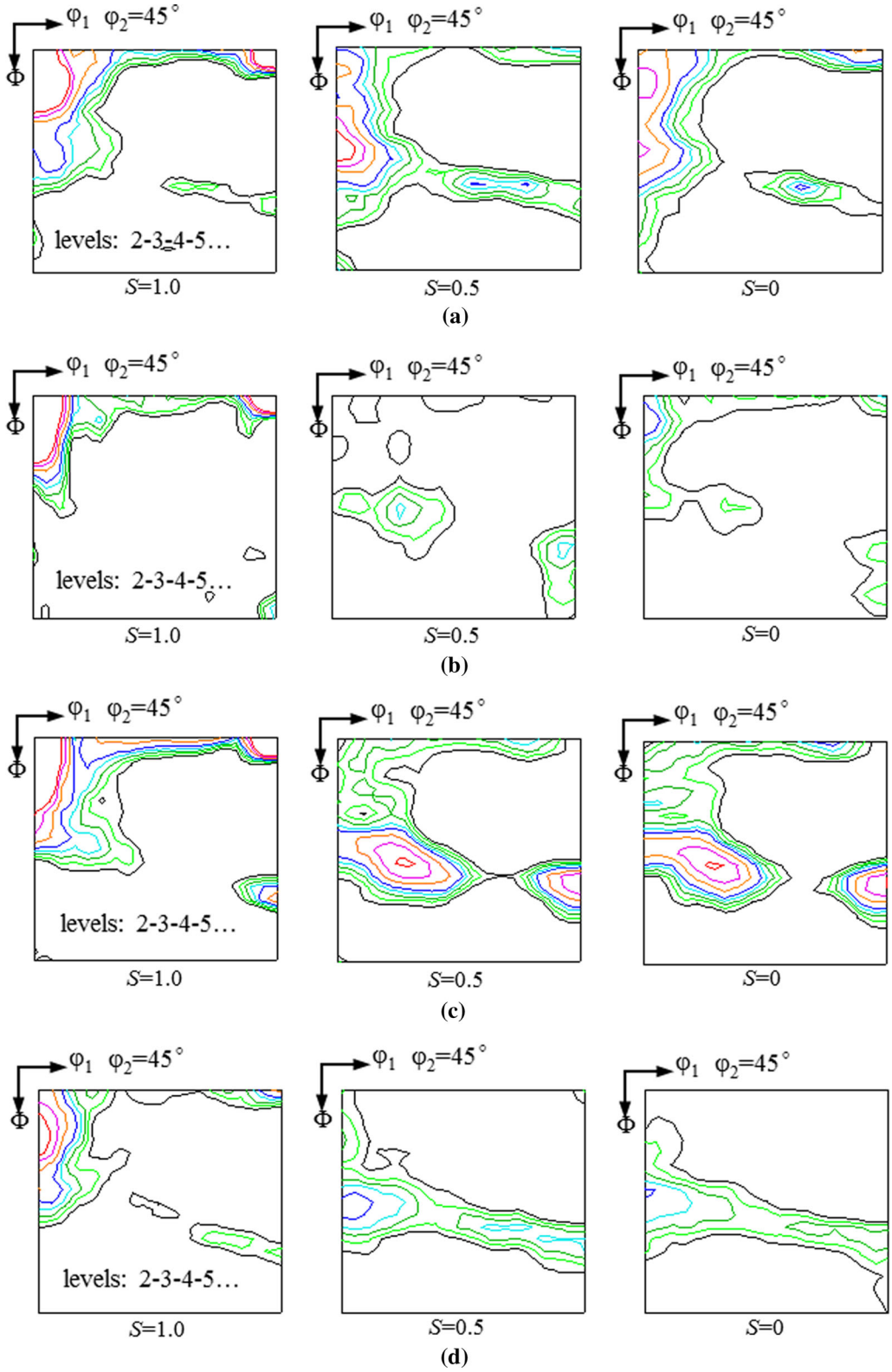

Fig. 8—Through-thickness textures ($\varphi_2 = 45$ deg section) of the strips which were processed by route R3. (*a*) First cold rolled strip, (*b*) intermediate annealed strip, (*c*) second cold rolled strip, and (*d*) primary annealed strip.

solidification. The newly formed MnS may take the existing AlN as nuclei to reduce Gibbs free energy and, thus, gave rise to the formation of lots of co-precipitates of AlN and MnS in the as-cast strip, as shown in Figure 9. During normalizing, the inhibitors were further precipitated to reduce the supersaturation of AlN

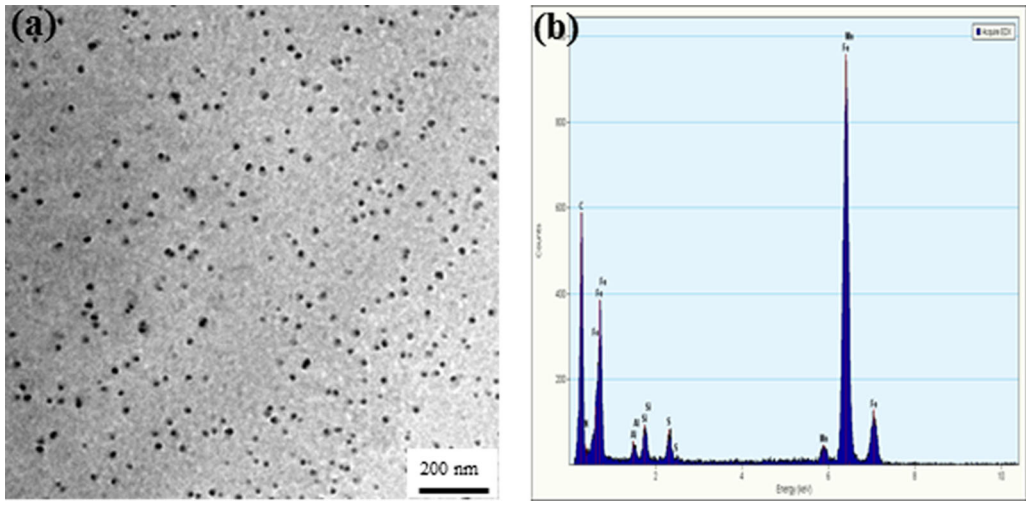

Fig. 9—TEM micrograph showing the inhibitors (*a*) and the typical EDXS spectrum (*b*) of the inhibitors in the as-cast strip.

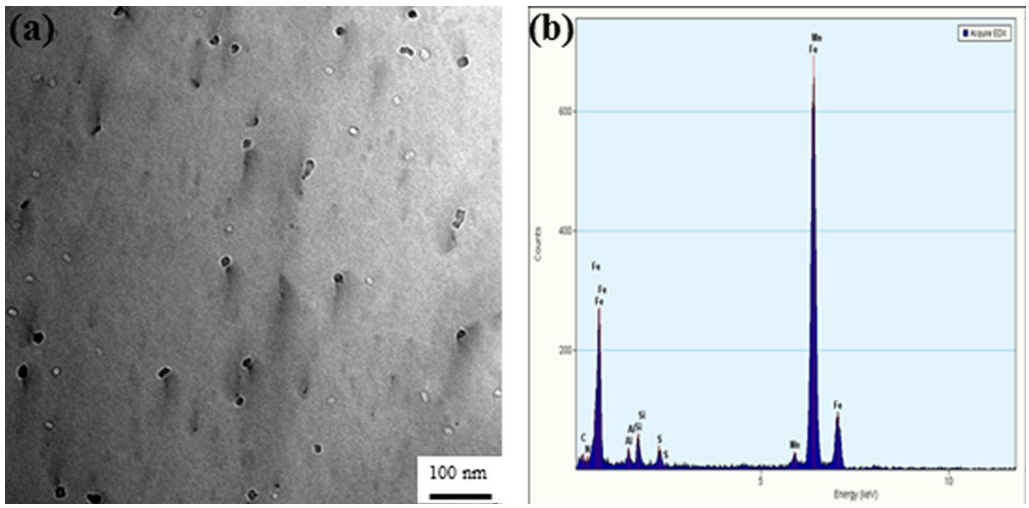

Fig. 10—TEM micrograph showing the inhibitors (*a*) and the typical EDXS spectrum (*b*) of the inhibitors in the normalized strip.

and MnS, and led to the increasing number and average size of inhibitors.

B. *Origin and Evolution of Goss Texture*

It is well accepted that Goss orientation originates due to shear deformation and Goss texture dominates below the hot rolled sheet surface.[9,19] And, hot rolling has a critical influence on the formation of final sharp Goss texture in conventional process.[20,21] However, despite the elimination of hot rolling in this work, relatively strong Goss texture was observed in the intermediate annealed strip (see Figure 7) and perfect secondary recrystallization microstructure was obtained (see Figure 11). Consequently, the origin and evolution of Goss texture may be considerably different from those in conventional process.

It was observed that Goss texture was absent in the as-cast strip and first cold rolled strip, as shown in Figures 2(b), 6(a), 7(a), and 8(a). However, after intermediate annealing, relatively strong Goss texture evolved through the whole thickness. After intermediate annealing, EBSD measurements showed that Goss grains were quite fine and located in banded colonies aligning at specific angles with respect to the rolling direction. These banded colonies composed of fine grains could be clearly observed in the intermediate annealed microstructures, as shown in Figures 3(b), 4(b), and 5(b). Dorothée Dorner *et al.*[22] investigated the texture evolution of an Fe3pctSi single crystal with Goss orientation and demonstrated that new Goss regions could be formed due to shear banding during cold rolling. Haratani *et al.*[23] reported that Goss grains are nucleated preferentially from shear bands in single crystals with $\{111\}\langle 112\rangle$ orientation and Fe-3pctSi polycrystalline samples. Ushioda *et al.*[24] observed that Goss grains are nucleated from shear bands in a 3 pct Si-Fe $\{111\}\langle 112\rangle$ single crystal. Jong-Tae Park *et al.*[25]

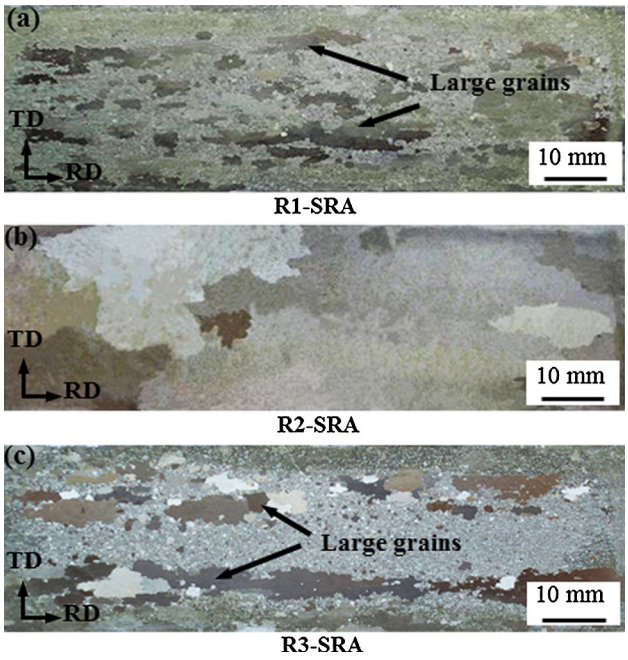

Fig. 11—Optical micrographs of the secondary recrystallization annealed strips which were processed by different routes. (*a*) R1-SRA strip, (*b*) R2-SRA strip, and (*c*) R3-SRA strip.

also reported that Goss grains are nucleated preferentially form shear bands in the deformed $\{111\}\langle 112\rangle$, $\{111\}\langle 110\rangle$, and $\{112\}\langle 110\rangle$ grains in 3 pct Si-Fe non-oriented silicon steel specimens. In this work, a portion of $\{111\}\langle 112\rangle$ component and lots of shear bands were observed in the first cold rolled state. Based on these observations in this work and the demonstrations in previous literatures, it could be inferred that Goss orientation had its origin within shear bands in the first cold rolling. However, because the Goss orientation within shear bands was quite weak, it could not be detected by X-ray diffraction, as shown in Figures 6(a), 7(a), and 8(a).

The nucleation within deformed grains is rapid where the stored energy is higher.[8] Shear bands are usually considered as the preferentially nucleation sites for new grains in the subsequently annealing due to higher stored energy than surrounding matrix. Consequently, the Goss orientation within shear bands may nucleate first and grow at the expense of the matrix and, thus, led to relatively strong Goss texture after intermediate annealing, as shown in Figures 6(b), 7(b), and 8(b). Because shear bands evolved through the whole thickness in the first cold rolled strips, Goss texture was also formed through the whole thickness after intermediate annealing. It should be noted that Goss texture in primary recrystallized state was quite weak in this work. This was greatly different from the results in which Goss texture was one of the populous primary recrystallization textures in two-stage route in conventional process.[8] This may be mainly related with different initial solidification structures and distinct processing routes.

Fig. 12—Optical microstructure showing the shear bands of the first cold rolled strip (R1-FCR) which was processed by route R1.

C. *Effects of Cold Rolling Schedule on Microstructure and Texture of Primary Annealed Strip*

It was shown that the as-cast strip was characterized by coarse columnar grains with strong λ-fiber texture. After first cold rolling, a remarkably inhomogeneous deformation microstructure composed of rough and smooth grains was observed. Figure 12 shows, the deformation microstructure of R1-FCR strip. As shown, all the rough grains and smooth grains showed sign of deformation in the form of lengthening. However, the rough grains exhibited dense deformation bands, while the smooth grains showed little sign of internal substructures. This microstructure inhomogeneity was considered to be closely related with the work hardening differences between grains with distinct initial orientations.[15] It should be noted that lots of shear bands (indicated by black arrows in Figure 12) were also clearly observed in some regions within rough grains. It is reported that shear banding is related to the mode of deformation such as activation of slip systems and strain hardening.[26] In this work, shear bands were observed in the cold rolled strips with thickness reduction of 56.5 to 73.9 pct. This fact supports the statement that shear bands after cold rolling more likely appear in the case of coarse-grained materials.[27–29] During intermediate annealing, the inhomogeneous deformation microstructures exhibited different nucleation and growth behavior due to various stored energy. It was known that the deformed $\{001\}\langle 0vw\rangle$ grains were difficult to recrystallize due to relatively low stored energy, while other deformed grains were easy to recrystallize as a result of high stored energy. Besides, under the intermediate annealing conditions applied in this work, the $\{001\}\langle 0vw\rangle$ grains could not be consumed by the growing grains which formed in the deformed grains with other orientations. As a result, an inhomogeneous microstructure with bi-model grain size distribution was produced, as shown in Figures 3(b), 4(b), and 5(b). As shown in Figure 13, the large elongated grains in primary annealed strips were all $\{001\}\langle 0vw\rangle$ oriented. It was observed that cold rolling schedule had a great influence on the primary annealed microstructure. As shown in Figure 4(d), the R2-PA strip showed a homogeneous microstructure composed of equiaxed grains through thickness. By contrast, some elongated grains evolved in R1-PA strip and R3-PA strip, as shown in Figures 3(d) and 5(d).

It was observed that cold rolling schedule had a significant effect on the texture evolution. Figures 6 through 8 show, the through-thickness textures of the strips and Figure 14 shows, the orientation densities along λ-fiber textures through thickness of the strips adopted by route 1 (R1). As shown, relatively strong λ-fiber textures evolved in the strips even after the cycle of first cold rolling, intermediate annealing and second stage cold rolling. After primary annealing, relatively strong λ-fiber textures still evolved at layers $S = 1.0$ and $S = 0.5$ in R1-PA strip and at layer $S = 1.0$ in R3-PA strip. This was in good agreement with the presence of elongated $\{001\}\langle 0vw\rangle$ oriented grains as shown in Figures 3(d), 5(d), and 13. The initial strong $\{001\}\langle 0vw\rangle$ solidification texture may be responsible for the evolution of relatively strong λ-fiber texture. Those $\{001\}\langle 0vw\rangle$ oriented grains in the primary annealed strips may be pernicious for the development of Goss texture during secondary recrystallization annealing. It should be noted that although the R1-PA and R3-PA strip showed medium λ-fiber texture, λ-fiber texture was almost absent in the R2-PA strip. This result indicated that appropriate cold rolling schedule may eliminate λ-fiber texture. Mishra *et al.*[9] pointed out that shear bands in cold rolled materials may contribute to the homogeneous recrystallization microstructure. The elimination of λ-fiber texture in R2-PA strip may be also related with those in-grain shear bands. It should be noted that R2-PA strip showed relatively strong γ-fiber texture through the whole thickness, while the R1-PA strip and R3-PA strip exhibited quite weak γ-fiber in the surface layer, as shown in Figure 15. This was closely related with the cold rolling schedules applied in this work and may have great effect on the secondary recrystallization.

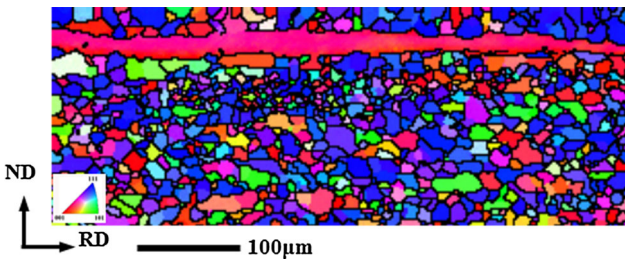

Fig. 13—Orientation image maps of all orientations on the longitudinal section of the primary annealed strip (R3-PA) which was processed by route R3.

D. *Effect of Microstructure and Texture of Primary Annealed Strip on Secondary Recrystallization*

It is known that dispersed inhibitors and suitable primary recrystallized structures are required for the formation of perfect secondary recrystallization microstructure.[8] In this work, although the inhibitor condition was identical, the SA strips adopted by different processing routes showed distinct microstructures. Thus, it might be concluded that the microstructure and texture in primary annealed state contributed to this remarkable difference.

It is reported that both potential Goss nuclei and the matrix should be optimally controlled in primary recrystallized state. The matrix should provide favorable surroundings for the abnormal growth of Goss grains during secondary recrystallization annealing and it is usually characterized by fine recrystallization grains and a suitable portion of $\{111\}\langle 112\rangle$ orientation.[8] In fact, the presence of certain amount of carbon benefits the formation of fine primary annealed grains with the help of γ/α transformation together with the inhibitors and

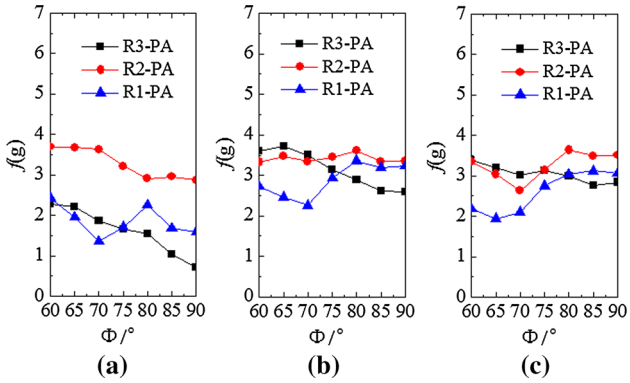

Fig. 15—Orientation densities along γ-fiber texture in surface layer (*a*), 1/4 layer (*b*), and center layer (*c*) of the primary annealed strip (R2-PA) which was processed by route R2.

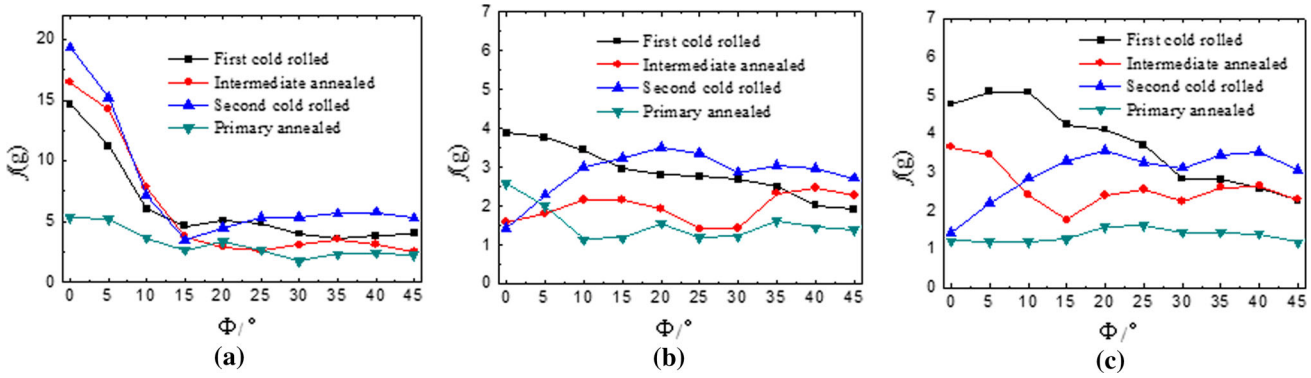

Fig. 14—Orientation densities along λ-fiber texture in surface layer (*a*), 1/4 layer (*b*), and center layer (*c*) of the strips which were processed by route R1.

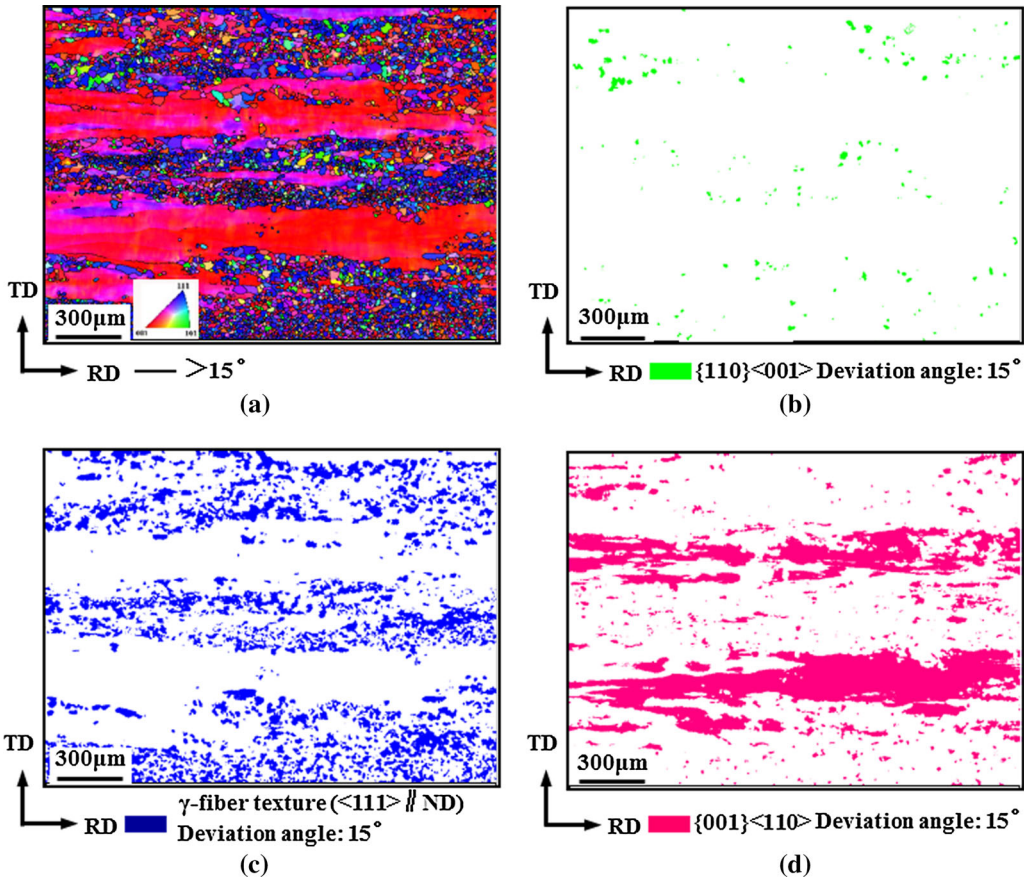

Fig. 16—Orientation image maps of all orientations (*a*), Goss orientation (*b*), γ-fiber orientation (*c*), and $\{001\}\langle 110\rangle$ orientation (*d*) on the subsurface of the primary annealed strip (R3-PA) which was processed by route R3.

carbides, although the cold rolled strips are usually annealed at a relatively high temperature [1108 K (835 °C) to 1123 K (850 °C)] for 4 to 5 minutes. In this work, the prevention of grain coarsening by γ/α transformation and carbides vanished because the tested steel remained in ferrite phase through the process. However, the combination of the relatively low annealing temperature, relatively short annealing time and high-density inhibitors in this work effectively prevented grain coarsening during primary annealing. Therefore, a fine microstructure was obtained, as shown in Figure 4(d). In this work, R2-PA strip showed a fine and homogeneous recrystallization microstructure with Goss texture, relatively strong γ-fiber texture and medium α-fiber texture through the thickness, as shown in Figures 7 and 15. After secondary recrystallization annealing, a perfect secondary recrystallization microstructure was produced, as shown in Figure 11(b). Consequently, it might be concluded that this combination of microstructure and texture is suitable for the formation of perfect secondary recrystallization in this work. It should be noted that although the magnetic induction of R1-SRA strip was 1.85 T, its core loss (1.43 W/kg) was relatively poor. It was observed that the R1-PA strip and R3-PA strip both exhibited inhomogeneous microstructure and weak γ-fiber texture. Some large elongated grains with λ-fiber texture were observed. Finally, the R1-SRA strip and R3-SRA strip both showed incomplete secondary recrystallization microstructure, as shown in Figures 11(a) and (c). The lack of Goss texture, the presence of weak γ-fiber and medium λ-fiber texture and the inhomogeneous microstructure may be responsible for the formation of incomplete secondary recrystallization. Therefore, the core losses of the R1-SRA and R3-SRA strips were quite poor ($P_{1.7/50} > 2.0$ W/kg). This combination of a few Goss grains and lots of fine grains with other orientations may be responsible for the poor core loss.

It was observed that all the large grains in R1-SRA strip and R3-SRA strip were elongated along the rolling direction. This may be related with the presence of large grains with λ-fiber texture in the primary annealed state. Figure 16 shows, the orientation image maps on the normal section of the R3-PA strip. It could be clearly observed that the strip was composed of two different types of regions. One type of region showed large grains with λ-fiber texture and the orientation was mainly $\{001\}\langle 110\rangle$, while the other type of region exhibited lots of fine grains with Goss orientation and γ-fiber texture. It could be inferred that, during the secondary recrystallization annealing, Goss grains in the region composed of fine grains may grow at the expense of the surrounding fine grains. However, the growth of Goss grains towards the transition direction may be blocked by the large $\{001\}\langle 110\rangle$ oriented grains due to the non-preferred misorientation. As a result, the large

grains were all elongated along the rolling direction and separated by fine grains.

From this work, it can be concluded that large $\{001\}\langle 0vw\rangle$ grains may still exist even after a long process of normalizing, two-stage cold rolling with an intermediate annealing and primary annealing on the condition of improper processing schedules (see Figures 3(d), 5(d), and 13). These $\{001\}\langle 0vw\rangle$ grains are very harmful to the development of Goss texture. It can be inferred that the initial fine grains with relatively random texture may be favorable to the formation of fine and uniform primary annealed grains and thus well-developed secondary recrystallization microstructure. In case of initial fine grains, the grain-oriented silicon steels with well-developed secondary recrystallization microstructure may be produced by the schedules with wide processing window or even one-stage cold rolling method, which remains as the future research subject.

V. CONCLUSIONS

The conclusions are summarized as follows:

1. A 0.27 mm-thick grain-oriented silicon steel sheet with extra-low carbon was successfully produced based on strip casting and two-stage cold rolling method. The magnetic induction of the secondary recrystallized sheet was as high as 1.85 T.
2. Goss texture originated in the first cold rolling due to shear banding. After intermediate annealing, relatively strong Goss texture evolved through the whole thickness.
3. Cold rolling schedule had a great influence on the microstructure and texture evolution and, thus, on the secondary recrystallization microstructure. When the cold rolling schedule was appropriate, the primary annealed strip showed homogeneous microstructure with Goss texture, relatively strong γ-fiber texture and medium α-fiber texture, leading to perfect secondary recrystallization and the magnetic induction B_8 was as high as 1.85 T.
4. In the case of inappropriate cold rolling schedules, inhomogeneous microstructure, weak γ-fiber texture and medium λ-fiber texture were observed in the primary annealed strip, which gave rise to incomplete secondary recrystallization microstructures.

ACKNOWLEDGMENTS

The authors gratefully acknowledge the financial support from National Natural Science Foundation of China (Grant Nos. 50734001, 51004035, 51374002, 51574078), the National Key Technology R&D Program (Grant No. 2012BAE03B00), the National High Technology R&D "863" Program (Grant No. 2012AA03A506), the Fundamental Research Funds for the Central Universities (Grant No. N140705001, N130607003), and the China Postdoctoral Science Foundation (Grant No. 2014M560218).

REFERENCES

1. T. Kubota, M. Fujikura, and Y. Ushigami: *J. Magn. Magn. Mater*, 2000, vol. 69, pp. 215–16.
2. N.P. Goss, U.S. Patent 1,965,559, 1934.
3. D. Senk, C. Schneider, and R. Kopp: *Steel Times Int*., 1991, vol. 14, p. 46.
4. K. Shibuya and M. Ozawa: *ISIJ Int*, 1991, vol. 31, pp. 661–668.
5. E.E.M. Luiten and K. Blok: *Energy Policy*, 2003, vol. 31, pp. 1339–56.
6. J.Y. Park, K.H. Oh, and H.Y. Ra: *Scripta Mater*., 1999, vol. 40, pp. 881–85.
7. C.G. Dunn: *Cold Working of Metals*, Cleveland, ASM, 1949, p. 113.
8. M. Matsuo: *ISIJ Int*., 1989, vol. 29, pp. 809–827.
9. S. Mishra, C. Darmann, and K. Lucke: *Acta Metall*., 1984, vol. 32, pp. 2185–201.
10. M. Matsuo, T. Sakai, and S. Yozo: *Metall. Trans*., 1986, vol. 17A, p. 1313.
11. A. Böttcher and K. Lücke: *Acta. Metall. Mater*., 1993, vol. 41, p. 2503.
12. A.A. Kononov and B.M. Mogutnov: *ISIJ Int*., 1999, vol. 39, pp. 64–68.
13. H.T. Liu, Z.Y. Liu, Y.Q. Qiu, G.M. Cao, C.G. Li, and G.D. Wang: *Mater. Charact*., 2009, vol. 60, pp. 79–82.
14. H. Liu, Z. Liu, C. Li, G. Cao, and G. Wang: *Mater. Charact*., 2011, vol. 62, pp. 463–68.
15. H. Liu, Z. Liu, G. Cao, C. Li, and G. Wang: *J. Magn. Magn. Mater*., 2011, vol. 323, pp. 2648–51.
16. H.T. Liu, Z.Y. Liu, Y. Sun, Y.Q. Qiu, C.G. Li, G.M. Cao, B.D. Hong, S.H. Kim, and G.D. Wang: *Mater. Lett*., 2012, vol. 81, pp. 65–68.
17. H.T. Liu, Z.Y. Liu, Y.Q. Qiu, Y. Sun, and G.D. Wang: *J. Mater. Process. Technol*., 2012, vol. 212, pp. 1941–45.
18. M.C. Tsai and Y.S. Hwang: *J. Magn. Magn. Mater*., 2010, vol. 322, pp. 2690–95.
19. Y. Shimizu, Y. Ito, and Y. Iida: *Metall. Trans A*, 1986, vol. 17A, pp. 1323–34.
20. C.G. Dunn: *Acta Metall*., 1953, vol. 1, p. 163.
21. S. Mishra, C. Darmann, and K. Lucke: *Metall. Trans A*, 1986, vol. 17A, pp. 1301–12.
22. D. Dorner, S. Zaefferer, and D. Raabe: *Acta Mater*., 2007, vol. 55, pp. 2519–30.
23. R. Haratani, B. Hutchinson, I.L. Dillamore, and P. Bate: *Metal Sci*., 1984, vol. 18, p. 57.
24. K. Ushioda and B. Hutchinson: *ISIJ Int*., 1989, vol. 29, p. 862.
25. J.T. Park and J.A. Szpunar: *Acta Mater*., 2003, vol. 51, pp. 3037–51.
26. M.Z. Quadir and B.J. Duggan: *Acta Mater*., 2006, vol. 54, pp. 4337–50.
27. K. Ushioda and W.B. Hutchinson: *ISIJ Int*., 1989, vol. 29, pp. 862–67.
28. M.D. Nave, M.R. Barnett, and H. Beladi: *ISIJ Int*., 2004, vol. 44, pp. 1072–78.
29. H.T. Liu, Z.Y. Liu, Y. Sun, F. Gao, and G.D. Wang: *Mater Lett*., 2013, vol. 91, pp. 150–53.